

# A Contact-Sliding-Triboelectrification-Driven Dynamic Optical Transmittance Modulator for Self-Powered Information Covering and Selective Visualization

Chen Zhang, Zihao Guo, Xiaoxiong Zheng, Xuejiao Zhao, Hailu Wang, Fei Liang, Song Guan, Ying Wang, Yongbin Zhao, Aihua Chen,\* Guang Zhu,\* and Zhong Lin Wang\*

Triboelectrification-enabled self-powered flexible electronic/optical systems have aroused a new surge of interest in recent years. All-in-one integration of such a system, which could significantly improve its adaptability, operability, and portability, still remains a challenge due to the absence of suitable architectures and integration schemes. Herein, a previously reported self-powered optical switch (OS) is thoroughly remolded and upgraded to a fully integrated contact-sliding-triboelectrification-driven dynamic optical transmittance modulator (OTM). The OTM is constructed with a multilayered structure, comprising a transparent triboelectrification top layer, a SiO<sub>2</sub>-spaced polymer dispersed liquid crystal (PDLC) intermediate layer, and a flexible transparent conductive substrate. The working mechanism is that an alternating electric field can be induced once contact-sliding occurs upon the OTM, rendering the PDLC layer immediately switching its initial translucent state to an instantaneous transparent state. As such, a decent dimming range with the relative transmitted light intensity from 0.17 to 0.72 can be achieved at low mechanical thresholds of contact pressure ( $\approx 20$  kPa) and sliding velocity ( $\approx 0.3$  m s<sup>-1</sup>). Moreover, for practical applications, demonstrations of information covering and selective visualization are successfully implemented without any extra optical elements nor external power supplies, explicitly showing great potential for the OTM in various self-powered optical interactive applications.

Flexible electronic/optical systems (FEOSs) emerging as a type of unprecedented and burgeoning integrated system have attracted tremendous attention over the past decades, owing to their revolutionary applications in electronic skins, portable/wearable/implantable devices, optical displays, and hybrid power packs.<sup>[1–6]</sup> The compelling demand for multifunctionality, higher performance, and lower power consumption of the FEOSs motivates people to make persistent efforts to develop new materials and architectures. In recent years, endowed with energy harvesting capabilities, self-powered FEOSs have aroused a new surge of interest, which can not only alleviate the battery replacement issues but also greatly enhance the sustainability, adaptability, operability and mobility of the FEOSs.<sup>[7–10]</sup> Especially, the triboelectric nanogenerator (TENG) as a booming energy-harvesting technology,<sup>[11]</sup> has proved to be an effective high-voltage source for driving various kinds of electrically

Dr. C. Zhang, Dr. X. X. Zheng, Dr. S. Guan, Prof. A. H. Chen  
School of Materials Science and Engineering  
Beihang University  
Beijing 100191, P. R. China  
E-mail: chenaihua@buaa.edu.cn

Dr. C. Zhang, Dr. Z. H. Guo, Dr. X. J. Zhao, Dr. H. L. Wang, Dr. F. Liang,  
Dr. Y. Wang, Prof. G. Zhu, Prof. Z. L. Wang  
CAS Center for Excellence in Nanoscience  
Beijing Key Laboratory of Micro-nano Energy and Sensor  
Beijing Institute of Nanoenergy and Nanosystems  
Chinese Academy of Sciences  
Beijing 100083, P. R. China  
E-mail: zhuguang@binn.cas.cn; zlwang@binn.cas.cn

Dr. Z. H. Guo, Dr. X. J. Zhao, Dr. H. L. Wang, Dr. F. Liang, Dr. Y. Wang,  
Prof. G. Zhu, Prof. Z. L. Wang  
School of Nanoscience and Technology  
University of Chinese Academy of Sciences  
Beijing 100048, P. R. China

 The ORCID identification number(s) for the author(s) of this article can be found under <https://doi.org/10.1002/adma.201904988>.

DOI: 10.1002/adma.201904988

Dr. Y. B. Zhao  
Shandong Oubo New Material Co. Ltd  
Dongying, Shandong 257088, P. R. China

Prof. A. H. Chen  
Beijing Advanced Innovation Centre for Biomedical Engineering  
Beihang University  
Beijing 100191, P. R. China

Prof. G. Zhu  
New Materials Institute  
Department of Mechanical  
Materials and Manufacturing Engineering  
University of Nottingham Ningbo China  
Ningbo 315100, P. R. China

Prof. G. Zhu, Prof. Z. L. Wang  
Center on Nanoenergy Research  
School of Physical Science and Technology  
Guangxi University  
Nanning 530004, P. R. China

Prof. Z. L. Wang  
School of Materials Science and Engineering  
Georgia Institute of Technology  
Atlanta, GA 30332, USA

responsive materials with diverse functions,<sup>[12,13]</sup> including electrochromism,<sup>[14]</sup> electroluminescence,<sup>[15–18]</sup> microfluidic control,<sup>[19–21]</sup> optical modulation,<sup>[14,22,23]</sup> electrostatic actuation,<sup>[24]</sup> and drug delivery,<sup>[25]</sup> among others. Nevertheless, these self-powered FEOSs generally consist of a discrete TENG and other functional devices, which may cause some inconvenience for their operations, placement, and carrying.<sup>[20,22,24]</sup> In this regard, all-in-one integration of such self-powered FEOSs becomes much needed and more adequate in order to satisfy some specific application circumstances.

Recently, our group developed a novel fully integrated motion-driven luminescence device based on triboelectrification-induced electroluminescence (TIEL) multilayered composites, showing great potential for dynamic and visualized sensing, such as position locating and motion tracking.<sup>[15]</sup> Afterwards, the resolution of the self-powered TIEL device was improved by inserting a transparent silver nanowires (AgNWs) electrode to guide and confine the spatial electric field vectors within the profile boundary of the contact object.<sup>[16]</sup> Moreover, we also integrated a lateral TIEL device through electrode geometry design to realize a pattern-customizable, large-scale, and flexible display for a variety of self-powered luminescence applications.<sup>[17]</sup> All above-mentioned progress demonstrates that directly integrating a triboelectrification layer onto the electric field responsive materials is a promising and technically feasible approach to fabricate all-in-one triboelectrification-enabled self-powered FEOSs.

In addition, we presented a self-powered optical switch (OS) more recently, which is similarly composed of a discrete surface-etched single-electrode TENG and a polymer-dispersed liquid crystal (PDLC) device.<sup>[26]</sup> The OS works by utilizing the output voltage of the TENG to trigger liquid crystal (LC) alignment in the PDLC device to rapidly switch its initial translucent state to an instantaneous transparent state. In this case, the PDLC device needs to be connected between the TENG's electrode and the ground so as to impose the output voltage upon itself. In other word, the OS seems more like a grounded mechano-electro-optical system rather than an individual free-standing device, which largely impairs its adaptability and portability. Therefore, in this work, we thoroughly remold and upgrade the OS to a fully integrated, contact-sliding-enabled, and self-powered flexible optical transmittance modulator (OTM). The OTM is constructed with a multilayered structure, comprising of a transparent fluorinated ethylene propylene (FEP) triboelectrification top layer, a SiO<sub>2</sub>-doped PDLC intermediate layer, and a flexible transparent poly(ethylene terephthalate)/indium tin oxide (PET/ITO) substrate. When a foreign object contact-slides on the FEP film, a real-time and rapidly changing electric field around the object can be induced by triboelectric charges, which could in turn continuously trigger LC alignment in the PDLC film. In this way, the initial light-scattering translucent state of the sliding area can be immediately and successively turned to an instantaneous light-transmitting transparent state along the sliding path (shown schematically in **Figure 1a**). As such, a decent dimming range with the relative transmitted light intensity from 0.17 to 0.72 can be achieved at a low threshold contact pressure of 20 kPa and a threshold sliding velocity of 0.3 m s<sup>-1</sup>. Since contact electrification is easily occurred and universally applicable to any material, the OTM can be effectively driven by

either insulating or conductive sliding materials, such as polyurethane (PU) sponge, nitrile rubber, nylon, aluminum foil, and even ordinary tissues. Moreover, for practical applications of the developed OTM, demonstrations of information covering and selective visualization are successfully carried out without any extra optical elements nor external power supplies. Considering that the OTM features other advantages in scalability, durability, response rate, cost, implementation, and portability, it therefore opens up a new paradigm for power-free optical modulation for various potential interactive applications, including privacy protection, electronic commerce, anticounterfeiting, trajectory tracking, and smart windows.

Figure 1b schematically illustrates the facile preparation process of the self-powered OTM. A moderate amount of PDLC solution containing SiO<sub>2</sub> spacers is first dropped onto a flexible PET/ITO substrate of 100 μm thick and gently covered with another PET substrate. It is then pressed under a stress of 20 N for 5 min to make the PDLC solution uniformly distributed with the thickness almost equal to the diameter of the SiO<sub>2</sub> spacers (≈20 μm), and it is subsequently cured under ultraviolet light (UV) of 365 nm. Lastly, a 50 μm thick FEP thin film is directly attached onto the cured PDLC film after removal of the top PET substrate (see details in Experimental Section). In this way, a multilayered structure is constructed for the OTM, as shown in **Figure 1c**. Note that the FEP film is used to produce triboelectric charges by sliding an object against its surface and its high transparency ensures that it would not cover up the electrically switchable light-scattering performance of the PDLC film (Note S1, Supporting Information).<sup>[15,17]</sup> Besides, according to our previous investigations on such layer-by-layer TIEL devices, an inserted conductive layer on PET substrate could significantly enhance the luminescence intensity by 90%, which is ascribed to the confined and converged spatial electric field.<sup>[15,16]</sup> Therefore, the PET/ITO conductive substrate in this case could also play a similar role in guiding and converging the spatial distribution of the electric field induced by triboelectric charges, which may make the electric field changes more dramatically and sharply while sliding taking place. As for the PDLC film sandwiched between the FEP film and PET/ITO substrate, it remains translucent all along in the absence of an external alternating electric field. In this state, the optical axis of each birefringent LC droplet is randomly oriented, as sketched in **Figure 1d**. It results in a spatially varying refractive index for the composite film because of the mismatch in polymer ( $\eta_p$ ) and droplet extraordinary ( $\eta_e$ ) refractive indices, and in turn causes the film to strongly scatter incident light in the forward direction. When an electric field is applied across the film, the LC molecules with positive dielectric anisotropy will realign their long axes parallel to the electric field direction. If the droplet ordinary refractive index ( $\eta_o$ ) matches  $\eta_p$  of the isotropic polymer matrix, the film will become transparent to normally incident light in this case.<sup>[27]</sup> Enabled by the unique electro-optical reaction, the initial translucent state at the sliding area of the OTM can be immediately switched to an instantaneous transparent state via a contact-sliding motion upon the FEP film (Video S1, Supporting Information). This is because an alternating spatial electric potential difference could be persistently induced around the sliding object during the process,<sup>[15–17]</sup> which is bound to be imposed on the nether

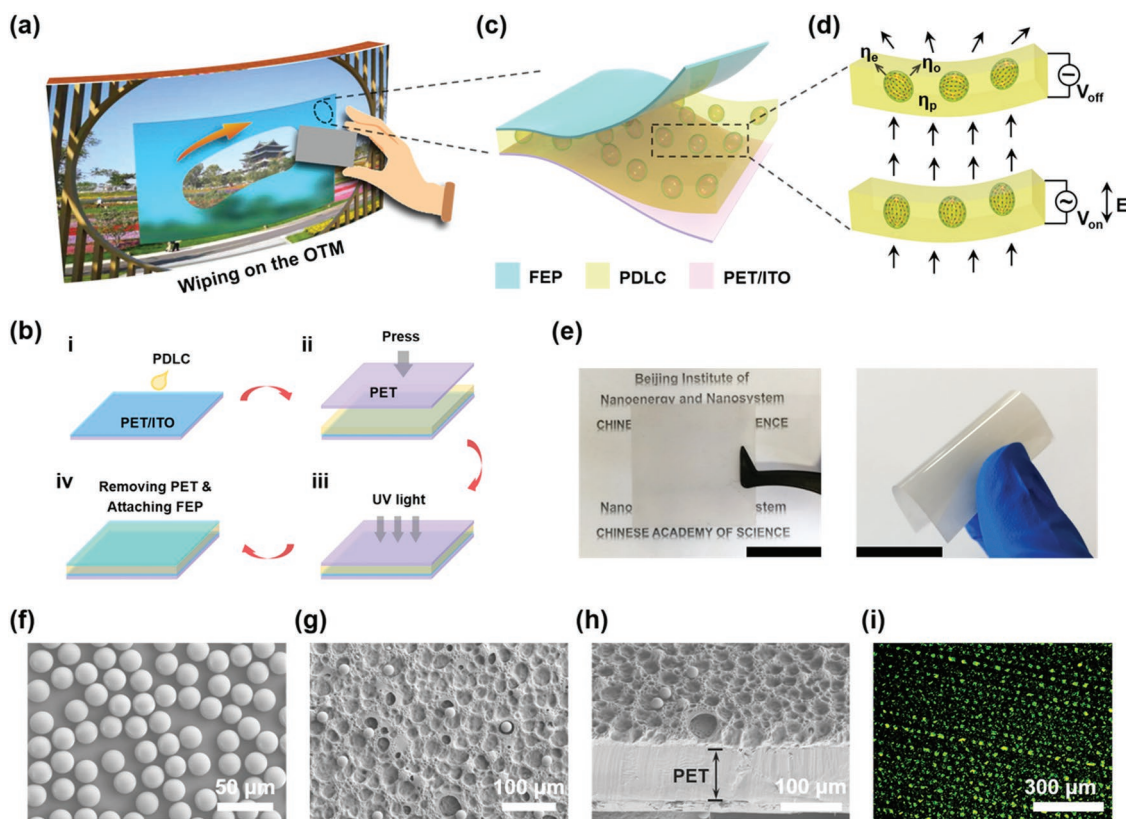


**Figure 1.** Structure of the self-powered OTM. a) Schematic diagram of the self-powered optical transmittance modulation enabled by contact-sliding-triboelectrification for the OTM. b) Schematic illustration of the fabrication process of the OTM. c) Schematic of layer-by-layer structure of the OTM. d) Cross-sectional view of locally magnified PDLC film. Approximately spherical birefringent LC droplets are dispersed within an isotropic polymer matrix. The light scattering can be switched off by simply applying an external electric field across the film to reorient the LC molecules in the droplets. e) Photographs of an as-fabricated OTM with a size of 5 cm × 5 cm placed 4 mm above a text and at bent state, respectively. The scale bar is 3 cm. f) SEM image of the SiO<sub>2</sub> spacers. g) Top-view and h) cross-sectional SEM images of the polymer network of the PDLC film. i) Optical image of the PDLC film under cross-polarization conditions.

PDLC film. In addition, enabled by the all-in-one and layer-by-layer structure, the OTM is fully capable of working independently, movably, and sustainably in the ambient environment, rendering a widespread applicability for numerous possible circumstances. Here, photographs that demonstrate the translucent state and bending flexibility of the OTM are respectively shown in Figure 1e. The text information placed 4 mm below the OTM can be completely shielded and becomes invisible, indicating decent light blocking effect and opacity of the OTM. In addition, Figure 1f–i presents scanning electron microscopy (SEM) images of the SiO<sub>2</sub> spacers and PDLC intermediate layer, respectively. The SiO<sub>2</sub> spacers are fairly uniform and its average diameter is ≈20 μm (Figure 1f). It enables the thickness of the PDLC film could be facily and evenly adjusted to ≈20 μm through sufficient pressure-retaining duration (Figure 1h). Besides, the polymer network of the PDLC film exhibits a porous structure with plenty of pits that correspond to dispersed LC droplets (Figure 1g), which can be clearly observed in the cross-polarization optical image as shown in Figure 1i. In our previous work, it was found that both threshold voltage and saturation voltage of the PDLC film decrease along with increasing the LC droplet diameter.<sup>[26]</sup> Therefore, here the PDLC film with micron-sized rather than nanoscaled LC droplets is

selected for constructing the self-powered OTM because of its relatively low threshold voltage and in order to obtain a better driving effect of the OTM.<sup>[26]</sup>

To further elaborate on the working mechanism and driving process of the self-powered OTM, numerical calculations are carried out by a finite element method (FEM) using COMSOL, as illustrated in Figure 2. The structure of the FEM model was built in three dimensions to accurately simulate the real working conditions and ensure the calculations more reliable (Figure 2a). As a result of contact-electrification between the sliding block and FEP film, equal amount of triboelectric charges with opposite sign are uniformly distributed on their surface, respectively.<sup>[28]</sup> In order to calculate the spatial distribution of the electric potential during the sliding process, the triboelectric charge density of the FEP film and sliding block surface needs to be estimated. Five types of block materials are utilized to slide on the FEP film at a velocity of 0.2 m s<sup>-1</sup>, respectively. After sufficient contact-sliding, the electric potential of the FEP film surface is found to be always negative, indicating an electron capture process for the FEP during the sliding process (Figure 2b). Moreover, Figure 2c,d, respectively, shows the short-circuit transferred charges ( $Q_{SC}$ ) between the ITO electrode of the OTM and the ground while the block

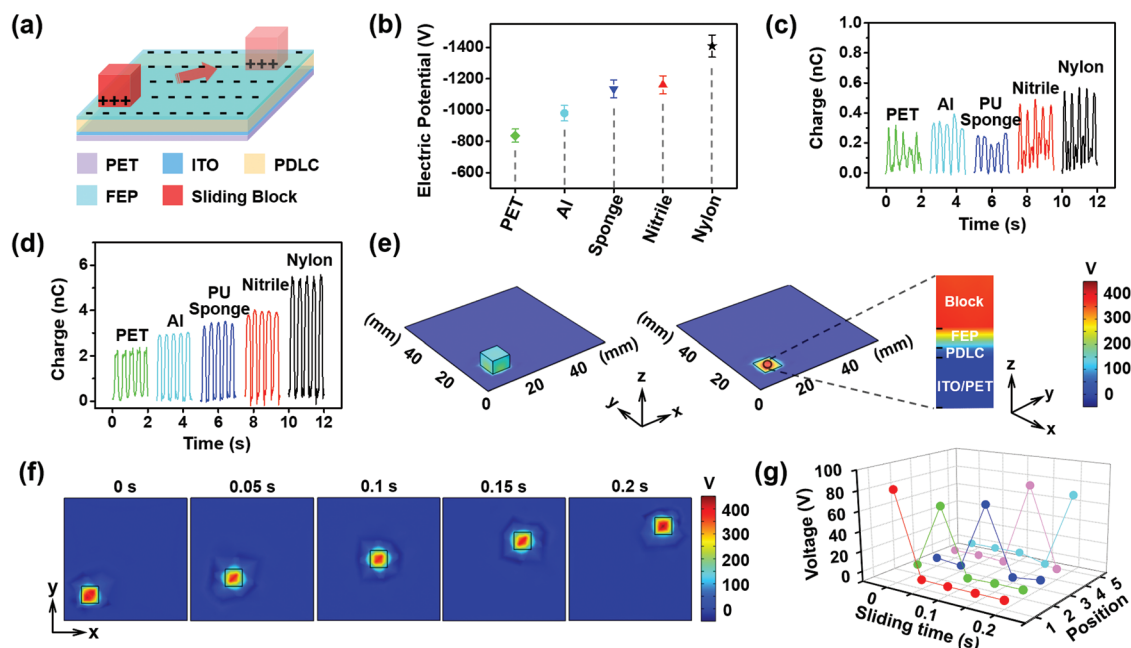


**Figure 2.** Theoretical analysis of the OTM. a) Structure model of the OTM for FEM simulation. b) Surface electric potential on the FEP triboelectrification layer after sufficient contact-sliding. c,d) Short-circuit transferred charges ( $Q_{SC}$ ) between the ITO electrode of the OTM and the ground while the block sliding inside the FEP area (c) and sliding in and out of the FEP area (d). e) The spatial distribution of the electric potential when the center of the nylon block is located at a coordinate point of (10.5, 10.5, 2.5). f) The electric potential distribution when the nylon block at five different places during it sliding along the diagonal direction. g) The corresponding top-down electric potential difference through the PDLC film during the sliding process.

sliding inside the FEP area and sliding in and out of the FEP area (Figure S1, Supporting Information). The corresponding short-circuit current ( $I_{SC}$ ) and open-circuit voltage ( $V_{OC}$ ) are also measured (Figure S2, Supporting Information). For the same block material, the amount of  $Q_{SC}$  is significantly larger as it sliding in and out of the FEP area than that as it only sliding inside the FEP area. This is due to that the farther the sliding block separates from the OTM, the weaker electrostatic interaction of the triboelectric charges between the FEP and sliding block would be.<sup>[24,28]</sup> In this case, the amount of generated triboelectric charges can be roughly regarded as the same as the  $Q_{SC}$  while the block sliding in and out of the FEP area. Based on these analyses, the nylon sliding block with the triboelectric charges of 5.5 nC is adopted for FEM calculations. Detailed simulation parameters are listed in Table S1 (Supporting Information). With the top surface of the FEP film as  $x$ - $y$  plane, Figure 2e shows special distribution of the electric potential when the center of the nylon block is located at a coordinate point of (10.5, 10.5, 2.5). It reveals that the electric potential around the interface between the nylon block and FEP film is remarkably higher than that elsewhere. In this state, top-down electric potential difference through the PDLC film (i.e., the electric potential difference between the bottom surface of the FEP film and top surface of ITO electrode) underneath the point of (10.5, 10.5, 0) is calculated to be 82 V (Figure 2e,g), which has already surpassed the threshold and saturation voltages of the PDLC film (discussed thereafter). Along the diagonal direction and at a velocity of  $0.2 \text{ m s}^{-1}$ , the nylon block could slide from the coordinate point of (10.5, 10.5, 2.5) to (38.5, 38.5, 2.5) in 0.2 s. Figure 2f presents the electric potential distribution of the  $x$ - $y$  plane when the nylon block at five

different places during the sliding process, respectively. The corresponding top-down electric potential difference through the PDLC film is also calculated and given in Figure 2g. The results indicate that the electric potential difference in a certain area would abruptly increase as the nylon block gets close to, and then dramatically decline when the nylon block leaves from. As a result, a sufficient alternating electric field could be successively produced in real time along the motion trajectory of the nylon block, and in turn makes the PDLC film simultaneously switch its light-scattering properties. In this way, facile and dynamic control of the light transmittance could be achieved by the developed OTM purely via simple contact-sliding motions.

To evaluate the electro-optical properties of the  $\text{SiO}_2$ -spaced PDLC film among the OTM, a counterpart device made of the PDLC film with two PET/ITO electrodes is adopted. The experimental setup is present in Figure S3 (Supporting Information). The counterpart device is driven by a sequence of external sinusoidal voltages at a frequency of 100 Hz (Figure 3a), which are derived from a function generator along with a linear amplifier. Figure 3b shows the measured spectra of transmitted light under different voltages as optical probe is tightly attached to the device. The corresponding transmittance at the wavelength of 404 nm is also intercepted (Figure 3c), which explicitly indicates that the threshold voltage and saturation voltage of the PDLC film are 10 and 50 V, respectively. Both of them are considerably lower than those of the PDLC with nanoscaled LC droplets.<sup>[26]</sup> At initial state, the relative intensity of the transmitted light ( $I_0$ ) is  $\approx 0.22$ , exhibiting decent light-scattering effect and opacity. At saturation voltage,  $I_0$  can reach up to a maximum value  $\approx 0.76$ , being adequate for a clear observation if any information is placed behind the device. In addition,

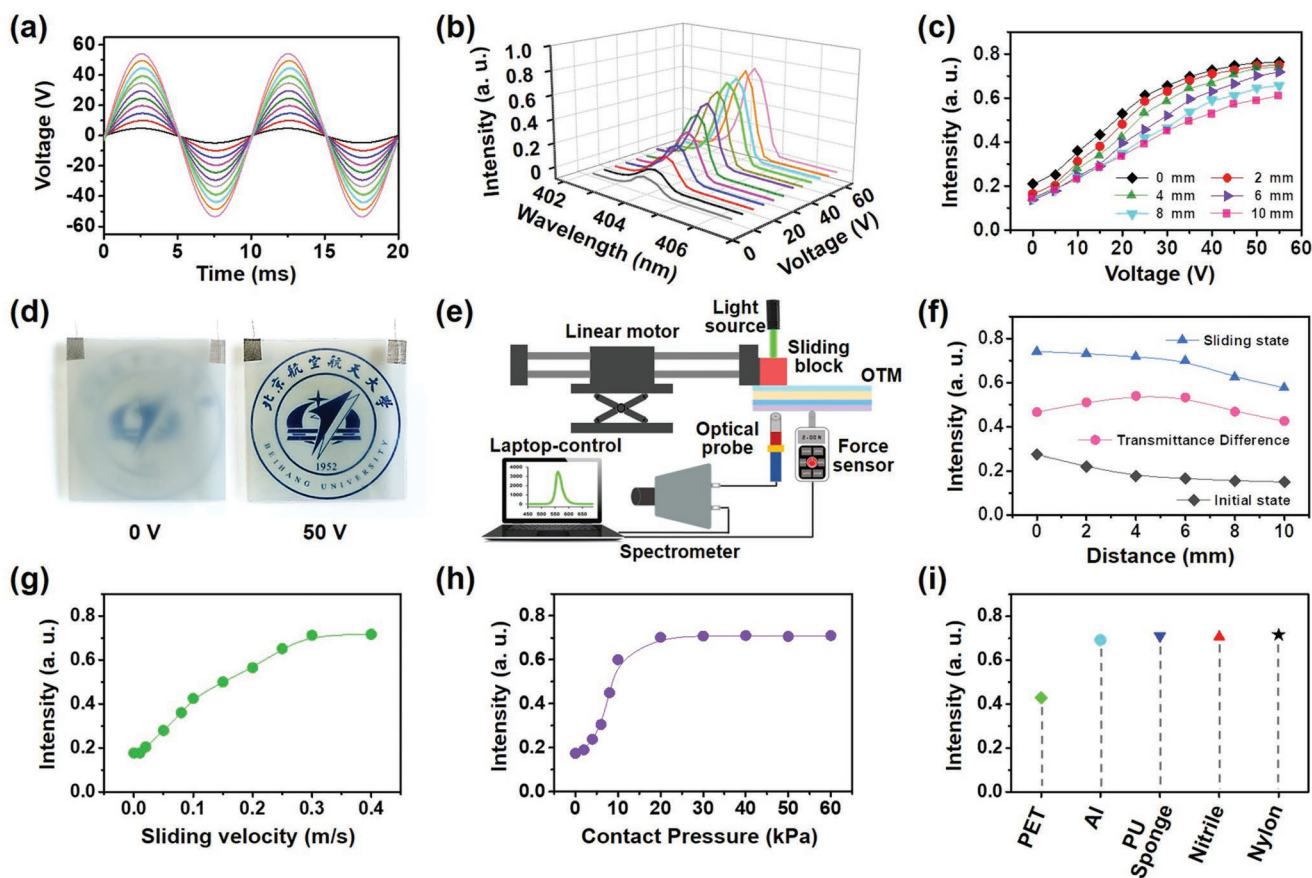


**Figure 3.** Experimental measurement results of the OTM. a) The sinusoidal voltages applied to a counterpart device with different magnitude at a frequency of 100 Hz. b) The spectra of the transmitted light under different voltages as the optical probe is tightly attached to the device. c) The relative intensity of the transmitted light under different voltages with varying the distance between the optical probe and the device. d) Photographs of an as-fabricated counterpart device (5 cm × 5 cm) placed 4 mm above a sign at 0 and 50 V, respectively. e) The schematic illustration of the test platform for measuring the mechano-optical performance of the OTM. f–h) The relative intensity of the transmitted light under initial and sliding states with varying distance ( $D_1$ ) between the optical probe and the OTM (f), and as a function of sliding velocity (g) and contact pressure (h), respectively. Here, the nylon is adopted as sliding block material. Notably, when one variable among  $D_1$ , sliding velocity, and contact pressure is in change, the other two are fixed. The corresponding fixed values are 4 mm,  $0.3 \text{ m s}^{-1}$  and 20 kPa, respectively. i) The responsiveness of the OTM upon different sliding block materials.

the transmitted spectra under different voltages are measured with varying the distance ( $D$ ) between the optical probe and the device (Figure 3c). It can be found that the  $I_0$  decreases with increasing  $D$  value in the whole voltage range, which is resulted from the haze of the device. Notably, the  $I_0$  could decrease faster by a little increase in  $D$  value at relatively low voltages (0–20 V), compared to that under saturation voltages. This is ascribed to the larger haze of the device at low voltages than that under saturation voltages. In this regard, Figure S4 (Supporting Information) provides the optical photographs of an as-fabricated counterpart device placed above a sign with different distances at initial (0 V) and saturation (50 V) state, respectively. At 0 V, the sign abruptly becomes fuzzy as the distance increases to 4 mm, whereas its definition at 50 V could not be obviously weakened until the distance reaches 10 mm. Therefore, the optimal distance between the information and the device can be roughly considered to be 4 mm, at which the information can be well sheltered or clearly visible through switching the light-scattering state of the PDLC film (Figure 3d, Figures S4 and S5, Supporting Information). Due to that only

the top PET/ITO electrode is replaced by a transparent FEP triboelectrification film, the optimal working distance of the OTM is believed to be the same as that of its counterpart device ( $\approx 4$  mm).

In this case, the mechano-optical performance of the OTM is further explored with respect to variables of contact-sliding velocity, contact pressure, and material category of the sliding block. Figure 3e schematically illustrates the test platform for the measurements. The sliding block is driven by a linear motor to controllably slide upon the FEP film of the OTM. At the same time, an optical probe is placed behind the OTM with variable distances ( $D_1$ ), and a force sensor is seamlessly attached to the OTM to detect the vertical force at the contact interface. At first, the nylon sliding block is utilized to slide on the FEP film at a contact pressure of 20 kPa and a sliding velocity of  $0.3 \text{ m s}^{-1}$  to measure the  $I_0$  value under initial and sliding conditions at different  $D_1$ , respectively. The result is well consistent with that of the counterpart device (Figure 3c,f), also suggesting the optimal working distance of the OTM is  $\approx 4$  mm. Then, with the  $D_1$  fixed to 4 mm, the mechano-optical response of the

OTM is studied in the light of different sliding velocity and contact pressure, respectively. As shown in Figure 3g, the  $I_0$  gradually increases with accelerating the sliding velocity almost in a linear manner, and saturates at a velocity of  $0.3 \text{ m s}^{-1}$ , revealing a strong motion frequency dependence for the OTM. In addition, rather low threshold contact pressure of 5 kPa and saturation contact pressure of 20 kPa are obtained (Figure 3h), which indicate that the OTM could be driven even by a very gentle contact at a certain sliding velocity. In the end, the responsiveness of the OTM upon five different types of block materials is analyzed (Figure 3i). The sliding blocks made of each material could well trigger the OTM to a saturation state except for PET, demonstrating a widespread applicability of the OTM possibly in many circumstances.

To transform the function of dynamic optical transmittance modulation into practical application for the OTM, demonstrations of self-powered information covering and selective visualization are carried out. As schematically illustrated in Figure 4a, the OTM is attached onto a transparent acrylic substrate with a thickness of 4 mm, which is placed seamlessly above a piece of text information. At initial state, the text is well covered by the raw OTM film, and then it can be facilely and selectively visualized via mechanical contact-sliding motions (Video S1, Supporting Information). Figure 4b–d shows the optical images (top row), corresponding color mapping images (middle row), and measured  $I_0$  values (bottom row) for the OTM at initial state and driven by nitrile rubber and tissue, respectively. The text underneath the OTM is completely fuzzy and unrecognizable (Figure 4b), yet it could immediately become clearly visible once a gentle contact-sliding motion occurs upon the OTM by a finger with nitrile glove (Figure 4c), and even by a piece of ordinary tissue (Figure 4d). From its corresponding color mapping images, the text at sliding area shows a darker color than elsewhere and the letters exhibit distinct outlines. Besides, the  $I_0$  value is also measured with a capture time of 200 ms. Although the light-transmitting is an instantaneous and reversible state

for the OTM, effective display of the text information can be still achieved through continuous sliding due to persistence of vision of human eyes (Video S1, Supporting Information). Moreover, the visible state of the OTM can be possibly prolonged by simultaneously extending the duration of triboelectrification-energy generation and decreasing the response frequency of the PDLC film due to its alternating responsive character. Likewise, the OTM can be also used to selectively visualize electronic tags, such as a 2D code, as shown in Figure 4e,f. There is a significant difference in definition of the code before and after contact-sliding on the OTM using a nylon film (Video S2, Supporting Information). As a result, instead of being unidentifiable with the shielding of the OTM film, the code can be immediately scanned out when contact-sliding occurs on the OTM (Video S3, Supporting Information). In addition, as a paradigm of self-powered mechano-optical modulator, the performance durability and reversibility of the OTM are considerably important for its practical applications. The relative intensity of the transmitted light from the OTM is collected over 5000 continuous cycles of contact-sliding motions by using a nylon block at a pressure of 20 kPa and a velocity of  $\approx 0.3 \text{ m s}^{-1}$ . As shown in Figure S6 (Supporting Information), the measurement interval is set to be 20 contact-sliding motion cycles. Almost no decay in transmitted light intensity of the OTM can be observed, which reveals its decent mechanical durability and optical reversibility. Considering that the OTM features other advantages in scalability, response rate, cost, implementation, and portability, it therefore opens up a new paradigm for self-powered optical modulation for various potential applications, such as privacy protection, electronic commerce, anticounterfeiting, trajectory tracking, and smart windows.

In summary, we have developed a sliding-mode triboelectric nanogenerator-enabled self-powered OTM based on triboelectrification-induced LC alignment in a PDLC film. In response to a gentle contact-sliding motion, the OTM is well capable of simultaneously and rapidly switching its initial translucent state

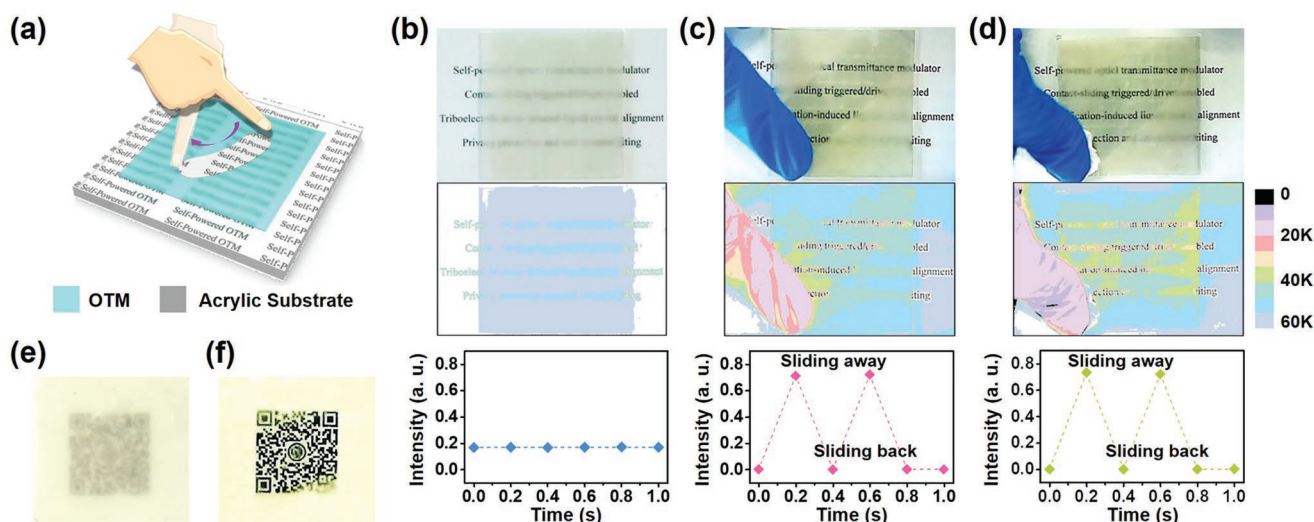


**Figure 4.** Demonstrations of the OTM for practical optical applications. a) Schematic diagram of the OTM for self-powered information covering and selective visualization. b–d) Optical images (top row), corresponding color mapping images (middle row), and relative intensity of the transmitted light (bottom row) for the OTM at initial state and driven by nitrile rubber and tissue, respectively. e, f) Optical images of a OTM-covered and contact-sliding-triboelectrification visualized 2D code, respectively.

to an instantaneous transparent state along the motion trajectory. This is due to that an alternating electric field could be successfully produced in real time by triboelectric charges during the sliding process, and in turn would exert a driving force upon the PDLC film. As such, a decent dimming range with the relative transmitted light intensity from 0.17 to 0.72 can be achieved at a low threshold contact pressure of 20 kPa and a threshold sliding velocity of  $0.3 \text{ m s}^{-1}$ . In addition, since contact electrification is easily occurred and universally applicable to any material, the OTM can be effectively driven by various sliding materials, rendering a widespread applicability possibly in many circumstances. More importantly, for practical applications, demonstrations of information covering and selective visualization are successfully carried out without any extra optical elements nor external power supplies. Our work may provide a novel approach toward the development of fully integrated, self-powered, and flexible optical devices for various possible interactive applications.

## Experimental Section

**Fabrication of the Self-Powered OTM:** An ITO layer with thickness of 150 nm was deposited on a flexible PET substrate of  $100 \mu\text{m}$  thickness as the transparent electrode. The uniform PDLC mixture was made by blending nematic liquid crystal E7 (Shenzhen Ma Gao Ding Chemical Plant) and photocurable polymer NOA65 (Norland Products) with a weight ratio of 60:40 (Figure S7, Supporting Information), and then adding 0.8 wt%  $\text{SiO}_2$  microspheres ( $\approx 20 \mu\text{m}$ ) as spacers. After vigorous stirring and ultrasonic bath at  $40^\circ\text{C}$  for 3 h, a moderate amount of PDLC solution ( $\approx 0.1 \text{ g}$  for an OTM device with a size of  $5 \times 5 \text{ cm}^2$ ) was dropped onto the PET/ITO substrate. In order to make the PDLC solution uniformly distributed with the thickness almost equal to the diameter of the  $\text{SiO}_2$  spacers, a robust PET substrate with  $150 \mu\text{m}$  thickness was used to gently cover the solution and then pressed under a stress of 20 N for 5 min. Subsequently, the multilayered structure was cured at room temperature under the UV light ( $\approx 365 \text{ nm}$ ) with a power density of  $1 \text{ mW cm}^{-2}$  for 15 min. At last, a FEP thin film of  $50 \mu\text{m}$  thickness was directly attached onto the cured PDLC film after removal of the top PET substrate.

**Characterization and Measurements:** The microstructure morphology of the  $\text{SiO}_2$  microspheres and the polymer network of the PDLC film were observed using a scanning electron microscope (SU8020, Hitachi). The LC droplet texture in the PDLC composite was observed via a polarizing optical microscope (59XF, Shang Guang). The mechano-electro-optical performance of the OTM was measured by low-noise voltage preamplifiers (Keithley 6514 System Electrometer and Stanford Research SR570) and a spectrograph (IsoPlane SCT320, Princeton Instruments). The in situ measurements were conducted by applying external AC voltages that derived from a function generator (DS345, Stanford Research Systems) along with a linear amplifier (WY605, NOLEPOWER). During the measurements, the OTM was attached to a transparent acrylic substrate and fixed to a stationary dam-board, whereas the sliding block was driven periodically by a linear motor and thus the contact-sliding motion can be precisely regulated.

## Supporting Information

Supporting Information is available from the Wiley Online Library or from the author.

## Acknowledgements

The authors gratefully acknowledge the financial support from the National Natural Science Foundation of China (Grant Nos. 51472018,

51272010, and 51572030), National Key R&D Project from Ministry of Science and Technology, China (Grant No. 2016YFA0202701 & 2016YFA0202703), Beijing Natural Science Foundation (Grant No. 2162047), Beijing Nova Program (No. XX2013009), Research Fund for the Doctoral Program of Higher Education (No. 20121102120001), and Fundamental Research Funds for the Central Universities (YWF-16-BJ-Y-75).

## Conflict of Interest

The authors declare no conflict of interest.

## Keywords

optical transmittance modulators, polymer-dispersed liquid crystals, selective visualization, self-powered devices

Received: August 2, 2019

Revised: October 21, 2019

Published online:

- [1] D. H. Kim, N. Lu, R. Ma, Y. S. Kim, R. H. Kim, S. Wang, J. Wu, S. M. Won, H. Tao, A. Islam, K. J. Yu, T. Kim, R. Chowdhury, M. Ying, L. Xu, M. Li, H. J. Chung, H. Keum, M. McCormick, P. Liu, Y. W. Zhang, F. G. Omenetto, Y. Huang, T. Coleman, J. A. Rogers, *Science* **2011**, 333, 838.
- [2] A. Chortos, J. Liu, Z. Bao, *Nat. Mater.* **2016**, 15, 937.
- [3] W. Gao, S. Emaminejad, H. Y. Y. Nyein, S. Challa, K. Chen, A. Peck, H. M. Fahad, H. Ota, H. Shiraki, D. Kiriya, D. H. Lien, G. A. Brooks, R. W. Davis, A. Javey, *Nature* **2016**, 529, 509.
- [4] Z. Zhang, L. Cui, X. Shi, X. Tian, D. Wang, C. Gu, E. Chen, X. Cheng, Y. Xu, Y. Hu, J. Zhang, L. Zhou, H. H. Fong, P. Ma, G. Jiang, X. Sun, B. Zhang, H. Peng, *Adv. Mater.* **2018**, 30, 1800323.
- [5] H. Ryu, H. J. Yoon, S. W. Kim, *Adv. Mater.* **2019**, 31, 1802898.
- [6] J. H. Park, S. Han, D. Kim, B. K. You, D. J. Joe, S. Hong, J. Seo, J. Kwon, C. K. Jeong, H. J. Park, T. S. Kim, S. H. Ko, K. J. Lee, *Adv. Funct. Mater.* **2017**, 27, 1701138.
- [7] Z. L. Wang, *Nano Energy* **2018**, 54, 477.
- [8] S. S. Kwak, H. J. Yoon, S. W. Kim, *Adv. Funct. Mater.* **2019**, 29, 1804533.
- [9] D. Y. Park, D. J. Joe, D. H. Kim, H. Park, J. H. Han, C. K. Jeong, H. Park, J. G. Park, B. Joung, K. J. Lee, *Adv. Mater.* **2017**, 29, 1702308.
- [10] J. Kim, P. Gutruf, A. M. Chiarelli, S. Y. Heo, K. Cho, Z. Xie, A. Banks, S. Han, K. I. Jang, J. W. Lee, K. T. Lee, X. Feng, Y. Huang, M. Fabiani, G. Grattton, U. Paik, J. A. Rogers, *Adv. Funct. Mater.* **2017**, 27, 1604373.
- [11] H. S. Wang, C. K. Jeong, M. H. Seo, D. J. Joe, J. H. Han, J. B. Yoon, K. J. Lee, *Nano Energy* **2017**, 35, 415.
- [12] J. Nie, X. Chen, Z. L. Wang, *Adv. Funct. Mater.* **2018**, 28, 1806351.
- [13] C. Wu, A. C. Wang, W. Ding, H. Guo, Z. L. Wang, *Adv. Energy Mater.* **2018**, 8, 1802906.
- [14] M. H. Yeh, L. Lin, P. K. Yang, Z. L. Wang, *ACS Nano* **2015**, 9, 4757.
- [15] X. Y. Wei, X. Wang, S. Y. Kuang, L. Su, H. Y. Li, Y. Wang, C. Pan, Z. L. Wang, G. Zhu, *Adv. Mater.* **2016**, 28, 6656.
- [16] Y. Wang, H. L. Wang, H. Y. Li, X. Y. Wei, Z. L. Wang, G. Zhu, *ACS Appl. Mater. Interfaces* **2019**, 11, 13796.
- [17] X. Y. Wei, H. L. Wang, Y. Wang, S. Y. Kuang, X. X. Zhu, J. Zou, L. Wang, X. Zeng, F. Rao, G. Zhu, *Nano Energy* **2019**, 61, 158.
- [18] H. J. Park, S. M. Kim, J. H. Lee, H. T. Kim, W. Seung, Y. Son, T. Y. Kim, U. Khan, N. M. Park, S. W. Kim, *ACS Appl. Mater. Interfaces* **2019**, 11, 5200.

- [19] J. Nie, Z. Ren, J. Shao, C. Deng, L. Xu, X. Chen, M. Li, Z. L. Wang, *ACS Nano* **2018**, *12*, 1491.
- [20] L. Zheng, Y. Wu, X. Chen, A. Yu, L. Xu, Y. Liu, H. Li, Z. L. Wang, *Adv. Funct. Mater.* **2017**, *27*, 1606408.
- [21] Z. H. Guo, Y. C. Jiao, H. L. Wang, C. Zhang, F. Liang, J. L. Liu, H. D. Yu, C. M. Li, G. Zhu, Z. L. Wang, *Adv. Funct. Mater.* **2019**, *29*, 1808974.
- [22] X. Chen, X. Pu, T. Jiang, A. Yu, L. Xu, Z. L. Wang, *Adv. Funct. Mater.* **2017**, *27*, 1603788.
- [23] C. Zhang, W. Tang, Y. Pang, C. Han, Z. L. Wang, *Adv. Mater.* **2015**, *27*, 719.
- [24] X. Chen, T. Jiang, Y. Yao, L. Xu, Z. Zhao, Z. L. Wang, *Adv. Funct. Mater.* **2016**, *26*, 4906.
- [25] P. Song, S. Kuang, N. Panwar, G. Yang, D. J. H. Tng, S. C. Tjin, W. J. Ng, M. B. A. Majid, G. Zhu, K. T. Yong, Z. L. Wang, *Adv. Mater.* **2017**, *29*, 1605668.
- [26] C. Zhang, H. L. Wang, S. Guan, Z. Guo, X. Zheng, Y. Fan, Y. Wang, T. Qu, Y. Zhao, A. Chen, G. Zhu, Z. L. Wang, *Adv. Funct. Mater.* **2019**, *29*, 1808633.
- [27] D. A. Higgins, *Adv. Mater.* **2000**, *12*, 251.
- [28] S. Niu, Y. Liu, S. Wang, L. Lin, Y. S. Zhou, Y. Hu, Z. L. Wang, *Adv. Funct. Mater.* **2014**, *24*, 3332.